THE JOURNAL OF
PHYSICAL CHEMISTRY A

ARTICLE

pubs.acs.org/JPCA

# A Single Chiroptical Spectroscopic Method May Not Be Able To Establish the Absolute Configurations of Diastereomers: Dimethylesters of Hibiscus and Garcinia Acids

Prasad L. Polavarapu,[†,*] Emily A. Donahue,[†] Ganesh Shanmugam,[†] Giovanni Scalmani,[‡] Edward K. Hawkins,[†] Carmelo Rizzo,[†] Ibrahim Ibnusaud,[§] Grace Thomas,[§] Deenamma Habel,[§] and Dellamol Sebastian[§]

[†]Department of Chemistry, Vanderbilt University, Nashville, Tennessee 37235, United States;

[‡]Gaussian, Inc., 340 Quinnipiac Street, Building 40, Wallingford, Connecticut 06492, United States

[§]Institute for Intensive Research In Basic Sciences, Mahatma Gandhi University, P.D. Hills PO, Kottayam, Kerala, India 686 560

S *Supporting Information*

**ABSTRACT:** Electronic circular dichroism (ECD), optical rotatory dispersion (ORD), and vibrational circular dichroism (VCD) spectra of hibiscus acid dimethyl ester have been measured and analyzed in combination with quantum chemical calculations of corresponding spectra. These results, along with those reported previously for garcinia acid dimethyl ester, reveal that none of these three (ECD, ORD, or VCD) spectroscopic methods, in isolation, can unequivocally establish the absolute configurations of diastereomers. This deficiency is eliminated when a combined spectral analysis of either ECD and VCD or ORD and VCD methods is used. It is also found that the ambiguities in the assignment of absolute configurations of diastereomers may also be overcome when unpolarized vibrational absorption is included in the spectral analysis.

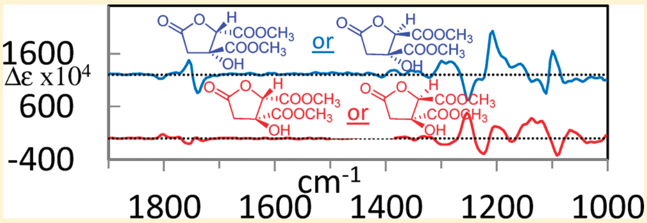

## INTRODUCTION

Hydroxycitric acids are widely utilized in medicines and food additives.[1] 1,2-Dihydroxypropane-1,2,3-tricarboxylic acid, or 2-hydroxycitric acid, **1** (see Chart 1) has two adjacent chiral centers and may exist in four stereoisomeric forms. The isolation of stereoisomers of **1** in their open chain forms is extremely difficult because the $\gamma$-hydroxyl group promotes spontaneous lactonization to a $\gamma$-butyrolactone ring system during isolation.[1] One of the lactone stereoisomers (see Chart 1), (2*S*,3*R*)-tetrahydro-3-hydroxy-5-oxo-2,3-furandicarboxylic acid, [(2*S*,3*R*)-**2**] is called hibiscus acid, and its diastereomer, (2*S*,3*S*)-tetrahydro-3-hydroxy-5-oxo-2,3-furandicarboxylic acid [(2*S*,3*S*)-**2**] is called garcinia acid. Both (2*S*,3*R*)-**2** and (2*S*,3*S*)-**2** are extensively distributed in nature,[2] but to the best of our knowledge no report is available on the existence of their enantiomers, (2*R*,3*S*)-**2** and (2*R*,3*R*)-**2**. Although hibiscus acid is extracted from the calyxes/leaves of *Hibiscus sabdariffa* (Mathippuli-Roselle plant), which is a common ingredient in many herbal tea blends, garcinia acid is extracted from the dried rind of the fruit of *Garcinia cambogia*, popularly known as "Malabar tamarind", and the latter has been credited for the unique regulatory role on fatty acid synthesis and weight loss.[3]

Since the absolute configurations of hibiscus and garcinia acids have been reported in the literature,[4] their known absolute configurations can be used to test the ability of chiroptical spectroscopic methods for predicting the absolute configurations. However, carboxylic acids are typically soluble in a limited number of polar solvents (i.e., water or dimethylsulfoxide), and therefore pose serious challenges for spectral interpretations. These challenges arise from the difficulties in theoretical modeling of molecular (solute−solvent) complexes, for which much progress remains to be realized. In the meantime, conversion of these acids to the corresponding dimethyl esters (see Chart 1), hibiscus acid dimethyl ester (HADE), (2*S*,3*R*)-**3** and garcinia acid dimethyl ester (GADE), (2*S*,3*S*)-**3**, allay these complications and make more straightforward the conformational search and the overall interpretation of the solvent effects, especially when an implicit solvent model is used.

The absolute configurations of chiral compounds containing heavy atoms can be determined using X-ray crystal structures. Chiroptical spectroscopic methods provide a convenient alternate route for determining the absolute configurations when a sample under investigation cannot be crystallized or a crystalline sample does not contain a heavy atom. Four chiroptical spectroscopic methods that have gained increased attention[5−8] in recent years include electronic circular dichroism (ECD),[5] optical rotatory dispersion (ORD),[5,6] vibrational circular dichroism (VCD),[5,7] and vibrational Raman optical activity (ROA).[5,8] The increasing interest in these methods is due to the reliability of their applications to chiral molecular structure determination

**Received:** March 16, 2011
**Revised:** April 28, 2011
**Published:** May 13, 2011

**Chart 1. Stereoisomers of 2-Hydroxycitric Acid, Corresponding Lactones and Their Dimethyl Esters**

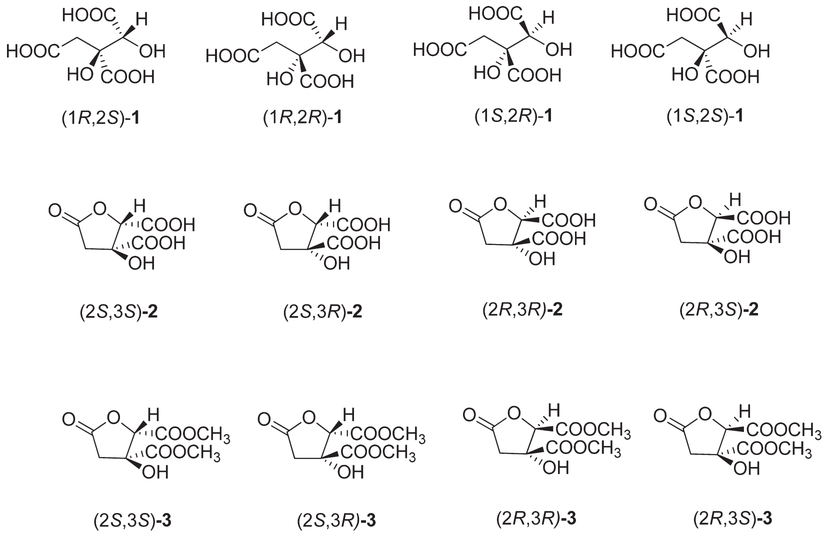

and the ease with which they can be applied to solution phase measurements. The availability of commercial instruments has made the routine experimental chiroptical spectroscopic measurements feasible, and recent advances in quantum chemical methods[5−8] have resulted in achieving improved accuracy for reliable predictions of chiroptical properties. Wider access to chiroptical spectroscopic instruments and to quantum chemical software that can calculate chiroptical properties, combined with improved computer technology for faster quantum chemical calculations, has made it convenient to apply chiroptical methods for determining the structures of chiral molecules ranging from small organic molecules to large natural products.[9]

If the absolute configuration of a chiral compound with a single source of chirality (such as a center of chirality or helical segment in the chiral molecule) is already known and the goal is just to verify if the predicted chiroptical spectra concur with the experimental spectra, one can calculate the chiroptical spectra for the known absolute configuration, using reliable quantum chemical methods and verify if the results compare well with the corresponding experimental spectra. Even if the absolute configuration of a chiral compound with a single element of stereochemistry is not known and the goal is to determine its absolute configuration, the quantum chemical calculation of chiroptical spectra for a chosen configuration is sufficient because those for its enantiomer are obtained by multiplying the calculated spectra by $-1$.

When a chiral compound has multiple elements of stereochemistry (multiple stereogenic centers or a combination of stereogenic centers and helical segments), one has to consider $2^n$ possible stereoisomers, where $n$ is the total number of stereochemical elements. In such cases, the procedure for determining or verifying the chiral molecular structures using chiroptical spectra is dependent on the following implicit criterion: If the experimentally observed chiroptical spectrum for an enantiomer of a chiral compound is satisfactorily reproduced by a quantum chemically predicted chiroptical spectrum for only *one* of all possible absolute configurations of that compound, then the absolute configuration used to calculate that satisfactorily predicted chiroptical spectrum can be assigned to the enantiomer used for experimental measurements. However, one cannot claim to have verified, or determined, the absolute configurations unequivocally if the quantum chemically predicted chiroptical spectra for *more* than one of the possible absolute configurations have a resemblance to the experimental spectrum. Therefore, if the goal is to determine the unknown absolute configurations of diastereomers unequivocally or to assess if a given chiroptical method can unequivocally verify the absolute configurations of diastereomers, then it is necessary to compare the predicted chiroptical spectra for all possible diastereomers with the experimental spectrum of a given enantiomer and ascertain that only *one* unequivocal match exists between predicted and experimental spectra. Unfortunately, this criterion is not strictly followed in the literature, because the predictive ability of a chiroptical spectrosopic method is often assessed by comparing *only* the predicted spectrum for the known configuration with the corresponding experimental spectrum. The presence/absence of any correlation between the predicted spectra for the other possible diastereomers and the experimental spectrum is not often verified.

For chiral compounds with multiple stereochemical elements, it is often the case that all of the diastereomers, or even more than a single diastereomer, are not available for experimental investigations. In such cases, it is not possible to experimentally determine if the diastereomers can even be distinguished from their chiroptical spectra. Thus, the compounds investigated here provide a unique opportunity, both experimentally and computationally, because two of the four diastereomeric compounds with known absolute configurations, namely HADE and GADE, are available for experimental investigations, and the remaining two are their enantiomers, which are expected to give mirror image chiroptical spectra. Thus, the experimental chiroptical data for all four diastereomers can be inferred and used to test the predictive, or discriminating, abilities of chiroptical spectroscopic methods.

We demonstrate in this study, using HADE and GADE as test cases, that a given chiroptical spectroscopic method by itself may not be able to unequivocally establish the absolute configurations of all diastereomers, but a combined analysis of the results from different chiroptical spectroscopic methods has a greater potential for a definite assignment of the absolute configurations. The role of unpolarized vibrational absorption spectra for discrimination among diastereomers is also analyzed.

## ■ PROCEDURES

**Experimental Section.** Hibiscus acid, isolated[1,10] from fresh leaves of *Hibiscus furcatus*/*Hibiscus sabdariffa*, was converted to HADE using diazomethane. An ethereal solution of diazomethane was prepared according to a literature procedure starting from *N*-nitroso-*N*-methylurea (1.6 g).[11] To a stirred solution of hibiscus acid (450 mg, 2.4 mmol) in methanol (3 mL), cooled in an ice bath, was added the ethereal diazomethane solution in small portions.[1] The gas evolution was allowed to subside between additions. The addition of diazomethane was continued until a faint yellow color persisted, indicating the reaction was complete, which was confirmed by TLC analysis (1:1 hexanes/ethyl acetate). The mixture was allowed to stand at room temperature until the yellow color faded, then the solvents were removed under reduced pressure. Purification was achieved by medium pressure liquid chromatography with a Biotage SP1 apparatus (Biotage, Charlottesville, VA) using a 25 × 75 mm 25+M cartridge with a flow rate of 25 mL/min, employing the following gradient: 100% methylene chloride for 1 column volume, 0−6% ethyl acetate in methylene chloride over 10 column volumes, 6% ethyl acetate in methylene chloride for 6 column volumes. HADE (278 mg, 1.3 mmol, 62%) was obtained as a yellow oil. NMR spectral data[12,13] were used to confirm the product. The isolation and preparation of garcinia acid and GADE were reported previously.[14]

The HADE and GADE samples used for experimental measurements will be referred to, respectively, as (+)-HADE and (+)-GADE, where (+) indicates positive optical rotation (at 589 nm in $CH_3CN$ solvent). Since the absolute configurations of hibiscus acid and garcinia acid are known[4] to be, respectively, (2*S*,3*R*) and (2*S*,3*S*), those of the corresponding esters will also be the same; that is, (2*S*,3*R*) for (+)-HADE and (2*S*,3*S*) for (+)-GADE. Thus, although (2*S*,3*R*)-**3** is the same as (+)-HADE and (2*S*,3*S*)-**3** is same as (+)-GADE, we will designate their experimental data as belonging, respectively, to (+)-HADE and (+)-GADE and calculated data for individual stereoisomers as belonging to (2*S*,3*R*)-**3**, (2*S*,3*S*)-**3**, (2*R*,3*S*)-**3**, or (2*R*,3*R*)-**3**.

The optical rotations at six discrete wavelengths (633, 589, 546, 436, 405, 365 nm) were measured at a concentration of 3 mg/mL in $CH_3CN$ and with a 0.5 dm cell using an Autopol IV polarimeter. The ORD spectra are presented as specific rotations (in units of deg cc $g^{-1}$ $dm^{-1}$)) as a function of wavelength (in units of nm). The electronic absorption (EA) and ECD spectra were recorded on a Jasco J720 spectrometer at a concentration of 7 mg/mL in $CH_3CN$ using a 0.01 cm path length quartz cell. The solvent spectrum has been subtracted from the experimental ECD spectrum of sample solution. The $CH_2Cl_2$ absorption prevents ECD measurements below ~230 nm; therefore, this solvent was not used for ECD measurements. The EA and ECD spectra are presented, respectively, as molar extinction and differential molar extinction, in units of L $mol^{-1}$ $cm^{-1}$, as a function of wavelength (in units of nm).

The vibrational absorption (VA) and VCD spectra were recorded in the 2000−900 $cm^{-1}$ region using a ChiralIR Fourier transform VCD spectrometer (BioTools, USA). The VCD spectra were recorded with 1 h data collection time at 8 $cm^{-1}$ resolution. VA and VCD spectra were measured in $CD_2Cl_2$ at a concentration of 1.8 mg/100 $\mu$L. The samples were held in a 100 $\mu$m fixed path length cell with $BaF_2$ windows. In the VA spectrum, the solvent absorption was subtracted. Similarly, the solvent VCD spectrum was subtracted from that of the sample solution. The ~1000−900 $cm^{-1}$ region has been excluded from presentation for the spectra measured in $CD_2Cl_2$ due to interference from $CD_2Cl_2$ absorption. The VA and VCD spectra are presented, respectively, as molar extinction and differential molar extinction, in units of L $mol^{-1}$ $cm^{-1}$, as a function of wavenumber (in units of $cm^{-1}$).

**Computational Details.** Since there are two stereogenic centers (each connected to a $COOCH_3$ group), four stereoisomers are possible for **3**, with two of them being mirror images of the other two. Calculations were performed for (2*S*,3*R*)-**3** and (2*S*,3*S*)-**3**. The chiroptical spectra for (2*R*,3*S*)-**3** and (2*R*,3*R*)-**3** were then generated from those of (2*S*,3*R*)-**3** and (2*S*,3*S*)-**3** by multiplying the latter by −1.

**VA and VCD Spectra.** For gas-phase VA and VCD calculations, optimized geometries were obtained using the B3LYP[15] functional and 6-31G*[16] and aug-cc-pVDZ basis sets.[17] VA and VCD calculations were performed at the respective optimized geometries and are designated as B3LYP/6-31G* and B3LYP/aug-cc-pVDZ. For VA and VCD calculations in $CD_2Cl_2$, geometries were reoptimized at the B3LYP/aug-cc-pVDZ level using the polarizable continuum model (PCM),[18] as recently modified[19] and implemented in the Gaussian 09 program.[20] VCD calculations using PCM were performed at the respective optimized geometries and are designated as B3LYP/aug-cc-pVDZ-PCM. Thus, the VA and VCD calculations performed at B3LYP/6-31G* and B3LYP/aug-cc-pVDZ represent gas phase results; those at B3LYP/aug-cc-pVDZ-PCM represent $CH_2Cl_2$ solution phase results. The theoretical VA and VCD spectra were simulated with Lorentzian band shapes of 10 $cm^{-1}$ half-width at half-peak height. Populations of conformers derived from Gibbs free energies were used to obtain the population-weighted VCD spectra.

**EA and ECD Spectra.** The predicted electronic transition energies obtained with the B3LYP functional are generally lower[21] than the corresponding experimental values. It has been shown that this deficiency may be corrected using the CAM-B3LYP functional,[22] which provides a better description of the tails of electronic density, by providing the correct asymptotic behavior of the exchange contribution. B3LYP and CAM-B3LYP functionals have similar accuracy for valence-type excitations, and CAM-B3LYP is clearly superior for Rydberg-type excitations.[21] Therefore, the CAM-B3LYP functional was also used with the aug-cc-pVDZ basis set for EA and ECD calculations. It is not necessary to use the fully optimized geometry for EA and ECD calculations at a given theoretical level, unlike for VCD calculations. Instead, for EA and ECD calculations at a higher level (including larger basis sets with diffuse functions), a geometry optimized at a lower level is deemed adequate. For this reason, the geometries were not reoptimized for CAM-B3LYP calculations, but those optimized in the B3LYP calculation were used. To provide a balanced view, it should be added that in using the CAM-B3LYP functional, although a larger exact-exchange contribution eliminates the ghost states,[23] the range-separated contribution may or may not work favorably,[24] depending on the size of the molecule (compared with the length scale that separates the short and long ranges). Calculations performed for EA and ECD are designated as B3LYP/6-31G*, B3LYP/aug-cc-pVDZ, and CAM-B3LYP/aug-cc-pVDZ to represent gas phase results and as B3LYP/aug-cc-pVDZ-PCM and CAM-B3LYP/aug-cc-pVDZ-PCM to represent $CH_3CN$ solution phase results. The theoretical EA and ECD spectra were simulated from the first 25 singlet → singlet electronic transitions using Gaussian band shapes and 15 nm half-width at 1/e of peak

Table 1. Dihedral Angles[a] of Optimized Conformers of (2*S*,3*R*)-3 (HADE) Ring Puckering

| | | | | B3LYP populations from internal energies[b] | | | |
|---|---|---|---|---|---|---|---|
| | | | | 6-31G* | aug-cc-pVDZ | | |
| conformer | ring-puckering angle ($O_{ring}-C_{ring}(=O)-C_{ring}-C_{ring}$) | $O{=}C-C_{ring}-O_{ring}$ | $O{=}C-C_{ring}-OH$ | gas | gas | $CH_3CN$[c]c | $CH_2Cl_2$[c]c |
| **1** | −19.2 | 175 | −0.47 | 0.36 | 0.37 | 0.25 | 0.30 |
| **2** | 15.2 | −36.5 | 12.7 | 0.25 | 0.26 | 0.13 | 0.16 |
| **3** | −19.6 | −153 | 178 | 0.16 | 0.12 | 0.03 | 0.04 |
| **4** | 14 | 139 | 11.9 | 0.15 | 0.18 | 0.05 | 0.08 |
| **5** | −17.9 | −3.4 | −0.6 | 0.07 | 0.07 | 0.51 | 0.39 |
| **6** | 12.4 | 151 | −144 | 0.01 | 0.01 | 0.00 | 0.00 |
| **7** | −17.9 | 7.2 | −177 | 0.00 | 0.00 | 0.04 | 0.03 |

[a] Dihedral angles provided here are those obtained from geometry optimizations at the B3LYP/6-31G* level. [b] Energies were obtained from reoptimized geometries with each basis set. [c] Using PCM.

height. Rotational strength values, calculated in the velocity representation, have been used for ECD spectral simulations. The EA spectral intensities have been derived from dimensionless oscillator strengths. Populations of conformers derived from the Gibbs free energies were used to obtain the population-weighted ECD spectra in the gas phase, and those derived from internal energies of PCM calculation using $CH_3CN$ as solvent were used to obtain the population-weighted solution phase ECD spectra.

**ORD Spectra.** The functionals and basis sets used for ORD calculation are identical to those used for ECD calculations. Optical rotations at six different wavelengths were calculated at the B3LYP/6-31G*, B3LYP/aug-cc-pVDZ, and CAM-B3LYP/aug-cc-pVDZ levels to represent gas phase results; and at the B3LYP/aug-cc-pVDZ-PCM and CAM-B3LYP/aug-cc-pVDZ-PCM levels to represent solution phase results.

VCD and ORD spectral calculations were performed using gauge-invariant atomic orbitals (GIAOs), and ECD spectral calculations were performed without using the GIAOs because ECD was calculated using the velocity formalism, which is origin-independent.

## RESULTS AND DISCUSSION

**Conformational Analysis.** Finding all possible low-energy conformations for cyclic ring molecules is a nontrivial task. For five-member ring molecules, in particular, it is necessary to undertake conformational analysis carefully.

*(2S,3R)-**3***. We used three different procedures to identify the low-energy conformers: (1) Manual search method. We built the plausible structures and began the geometry optimizations using the Gaussian 09 program[20] at the STO-2G level. To obtain all possible conformations, the positive puckering angles of four different optimized conformations were changed to negative values, and eight geometries were reoptimized at the B3LYP/6-31G* level. However, the negative puckering values reverted back to the positive puckering angles during optimization. Therefore, this type of conformational search required maintaining the ring-puckering value as a constant (or performing a potential energy scan by varying the rest of the structural parameters) or determining the remaining plausible conformations by other means (see below). In the end, we arrived at the conformations listed in Table 1. To ensure that all possible conformations had been identified, we then used two different conformational search programs as described below. (2) Conformational search using SPARTAN program.[25] When default options are used,[26] this program searches for conformations by changing the torsional angles of rotatable bonds, but does not look for conformations that differ in the signs of ring-puckering torsional angles[27] in the conformational search. As a consequence, the inversion of the ring-puckering angle (that is, a change in the sign of the ring-puckering torsional angle) could not be realized. For this reason, one geometry with a positive puckering torsional angle and a second geometry with a negative puckering torsional angle were separately used as starting geometries to find low-energy conformers within 20 kcal/mol energy range. This procedure resulted in 11 conformations with positive puckering torsional angles and 13 conformations with negative puckering torsional angles. These 24 conformations were further optimized at the B3LYP/6-31G* level, and seven lowest energy conformations (see Table 1) were selected for further consideration. (3) Conformational search using the CONFLEX program.[28] This program by default looks for conformations that differ in the signs of ring-puckering torsional angles.[29] Three different starting geometries of HADE, each with a different positive or negative puckering torsional angle, were used for the conformational search within a 20 kcal/mol energy range. All three cases yielded the same set of 19 conformations. These 19 conformations were optimized at the B3LYP/6-31G* level, which led to the same seven lowest energy conformations that are included in Table 1. For solution phase predictions, the low-energy conformers found in the gas phase were reoptimized using PCM.[19,20]

It is important to note that there are significant differences in populations of gas-phase and solution-phase conformers. For example, at the B3LYP/aug-cc-pVDZ level, conformer **5** has a population of 7% in gas phase and 51% in $CH_3CN$. This observation emphasizes the importance of using PCM,[19,20] as noted previously,[14] to interpret the solution phase chiroptical data.

*(2S,3S)-**3***. The conformers of GADE were determined previously[14] using a manual search method. Four different structures with positive puckering angles were built and optimized at the B3LYP/631G* level. The resulting geometries were reoptimized at the B3LYP/aug-cc-pVDZ level, then the puckering angle in each of the conformers was manually changed to a negative value and reoptimized, leading to a total of eight conformers in the gas phase. Among these eight conformers, six conformers are within 2 kcal/mol. For solution phase predictions, the low-energy conformers

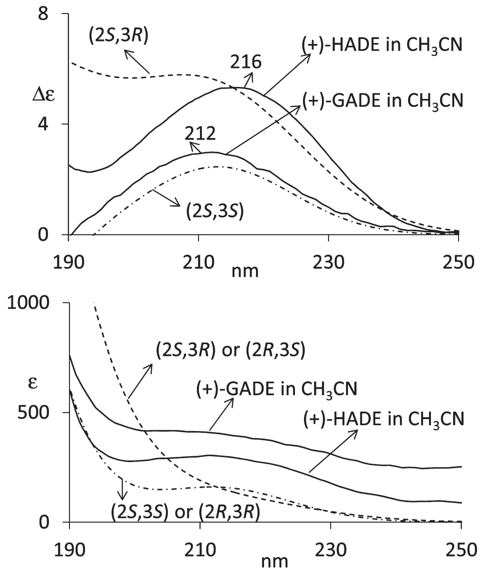

**Figure 1.** Experimental EA (bottom) and ECD (top) spectra for dimethylesters of hibiscus acid (HADE) and garcinia acid (GADE) in $CH_3CN$ and population-weighted corresponding spectra obtained at the CAM-B3LYP/aug-cc-pVDZ-PCM level for (2*S*,3*R*)-**3** and (2*S*,3*S*)-**3** diastereomers.

found in the gas phase were reoptimized using PCM. In addition to this method, we also used a conformational search using the CONFLEX program[28] (with the same options[29] as used for HADE). The conformational search for GADE yielded 13 conformations. These 13 conformations were further optimized at the B3LYP/6-31G* level, which led to the same six low-energy conformers[14] as found in the above-mentioned manual search method.

In summarizing the conformational analysis section, the use of multiple procedures that use different criteria for a conformational search, and augmenting a conformational search with potential energy scans, provides confidence that an employed conformational search procedure may not have missed any low-energy conformations. Therefore, this multiprong approach appears suitable to being adopted as a part of the standard protocol for conformational analysis.

It is to be cautioned that, even though the conformational search description given above for HADE and GADE may appear to favor the use of the CONFLEX program,[28] we found this program not to be suitable for conducting the conformational search for salts of carboxylic acids. The conformational analysis of chiral carboxylic acid salts will be communicated in the near future.

**EA and ECD Spectra.** The experimental ECD spectra for (+)-HADE and (+)-GADE in the 190−250 nm region are shown in Figure 1. The experimental EA spectra of (+)-HADE and (+)-GADE are similar in the 190−250 nm region: both have a weak and broad absorption band spanning the 200−230 nm region. In the ECD spectra of (+)-HADE and (+)-GADE, there is only one positive ECD band each (at 216 nm for HADE and at 212 nm for GADE). The magnitude of observed $\Delta\varepsilon$ is larger for (+)-HADE than that for (+)-GADE.

The predicted population-weighted EA and ECD spectra for (2*S*,3*R*)-**3** at the CAM-B3LYP/aug-cc-pVDZ-PCM level are shown in Figure 1, and the rest are provided as the Supporting Information. The predicted ECD spectra at the B3LYP/631G*, B3LYP/aug-cc-pVDZ, B3LYP/aug-cc-pVDZ-PCM, and CAM-B3LYP/aug-cc-pVDZ-PCM levels display one well-defined positive ECD band in the 190−250 nm region. In the predicted spectrum at the CAM-B3LYP/aug-cc-pVDZ level (see Supporting Information), this positive ECD band occurs below 190 nm, and only the long wavelength tail of this positive ECD band can be seen in the 190−250 nm region. Thus, the sign of the predicted ECD band in the 190−250 nm region for (2*S*,3*R*)-**3** concurs with experimental observation for (+)-HADE at all levels of calculations undertaken. Quantum chemical calculations of EA and ECD spectra for (2*S*,3*S*)-**3** were reported,[14] and the importance of using the recent implementation[19,20] of PCM for predicting the correct ECD sign was discussed. The predicted population-weighted EA and ECD spectra for (2*S*,3*S*)-**3** at the CAM-B3LYP/aug-cc-pVDZ-PCM level are also shown in Figure 1.

**Table 2. Absolute Configurations Inferred from Individual Spectroscopic Methods**

| method | (+)-HADE[a] | | (+)-GADE[a] | |
|---|---|---|---|---|
| ECD | **(2*S*,3*R*)** | (2*S*,3*S*) | (2*S*,3*R*) | **(2*S*,3*S*)** |
| ORD | **(2*S*,3*R*)** | (2*S*,3*S*) | (2*S*,3*R*) | **(2*S*,3*S*)** |
| VCD | **(2*S*,3*R*)** | (2R,3R) | (2R,3S) | **(2*S*,3*S*)** |
| VA | **(2*S*,3*R*)** | (2R,3S) | (2R,3R) | **(2*S*,3*S*)** |

[a] Bold entries represent common configrations predicted by all spectroscopic methods.

In summarizing this section, the predicted ECD spectra of (2*S*,3*R*)-**3** and (2*S*,3*S*)-**3** in the 190−250 nm region are similar, as are the experimental ECD spectra of (+)-HADE and (+)-GADE. Except for minor differences in band positions and peak intensities, these ECD spectra are not very useful for differentiating between the (2*S*,3*R*)-**3** and (2*S*,3*S*)-**3** diastereomers. Since the enantiomers, (2*R*,3*S*)-**3** and (2*R*,3*R*)-**3**, would have ECD spectra with signs opposite to those of (2*S*,3*R*)-**3** and (2*S*,3*S*)-**3**, respectively, ECD spectra are also not useful for differentiating between the (2*R*,3*S*)-**3** and (2*R*,3*R*)-**3** diastereomers.

The EA spectra of enantiomers will be the same, but those of diastereomers need not be the same. However, the predicted EA spectra of (2*S*,3*R*)-**3** and (2*S*,3*S*)-**3** diastereomers, as also seen in the experimental spectra of (+)-HADE and (+)-GADE, are similar. Therefore, the EA spectra in the 190−250 nm region are also not useful for differentiating between (2*S*,3*R*)-**3** and (2*S*,3*S*)-**3** diastereomers. Therefore, if the absolute configurations of (+)-HADE and (+)-GADE were not known, then on the basis of quantum chemical calculations of ECD, one could associate either (2*S*,3*R*) or (2*S*,3*S*) configurations to each of them (as summarized in Table 2). As a consequence, ECD spectra (either alone or in combination with EA spectra) in the 190−250 nm region cannot unequivocally determine the absolute configurations of diasteromers of **3**.

**ORD Spectra.** The experimental ORD spectra for (+)-HADE and (+)-GADE are shown in Figure 2. The optical rotations are positive for both HADE and GADE at all six wavelengths examined. The differences among them are only in magnitude, with specific rotations of HADE being slightly larger than those of GADE. These experimental data indicate that experimental ORD is not very useful to differentiate between the (2*S*,3*R*) and (2*S*,3*S*) diastereomers (and also between the corresponding enantiomers).

The predicted population-weighted ORD spectra for (2*S*,3*R*)-**3** at the CAM-B3LYP/aug-cc-pVDZ-PCM level are shown in Figure 2, and the rest are provided as Supporting Information.

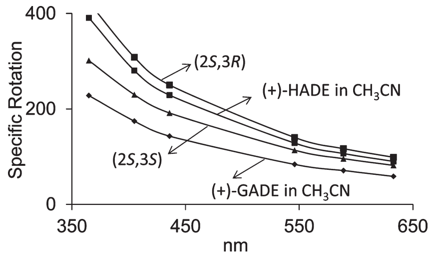

**Figure 2.** Experimental ORD spectra for (+)-HADE and (+)-GADE in $CH_3CN$ and population-weighted ORD spectra obtained at the CAM-B3LYP/aug-cc-pVDZ-PCM level for (2*S*,3*R*)-**3** and (2*S*,3*S*)-**3** diastereomers.

The predicted ORD spectra at all theoretical levels display positive rotations at all six wavelengths calculated. Thus, the signs of predicted rotations for (2*S*,3*R*)-**3** at all levels of calculations undertaken concur with experimental observation for (+)-HADE. The same observation holds for (+)-GADE; quantum chemical calculations of ORD spectra for (2*S*,3*S*)-**3** were reported and discussed previously.[14] The predicted population-weighted ORD spectrum for (2*S*,3*S*)-**3** at the CAM-B3LYP/aug-cc-pVDZ-PCM level is shown in Figure 2.

In summarizing this section, the predicted ORD spectra of (2*S*,3*R*)-**3** and (2*S*,3*S*)-**3** in the 365−633 nm region are similar, as are the experimental ORD spectra of (+)-HADE and (+)-GADE. Except for minor differences in the magnitude of the specific rotations, ORD spectra are not useful for differentiating between the (2*S*,3*R*)-**3** and (2*S*,3*S*)-**3** diastereomers. Since (2*R*,3*S*)-**3** and (2*R*,3*R*)-**3** are enantiomeric to (2S,3R)-**3** and (2S,3S)-**3**, respectively, their ORD spectra would have opposite signs and are not useful for differentiating between the (2*R*,3*S*)-**3** and (2*R*,3*R*)-**3** diastereomers. Therefore, if the absolute configurations of (+)-HADE and (+)-GADE were not known, then on the basis of the quantum chemical calculations of ORD, in the 365−633 nm region, one could associate either (2*S*,3*R*) or (2*S*,3*S*) configurations to each of them (as summarized in Table 2). As a consequence, ORD spectra in the 365−633 nm region, by themselves, cannot unequivocally determine the absolute configurations of diasteromers of **3**.

**VA and VCD Spectra.** The experimental VA and VCD spectra for (+)-HADE and (+)-GADE in the 1900−1000 $cm^{-1}$ region are shown in Figure 3. Unlike EA spectra, the experimental VA spectra of (+)-HADE and (+)-GADE are quite different. Similarly, the VCD spectra of (+)-HADE and (+)-GADE are also quite different, which is in contrast to the ECD spectra. The experimental VCD bands originating from the C=O stretching modes (1800−1700 $cm^{-1}$ region) have opposite signs for (+)-HADE and (+)-GADE (although the magnitudes of VCD intensities in (+)-GADE are much smaller). Similarly, the experimental VCD bands at ∼1300 and 1254 $cm^{-1}$ have opposite signs in (+)-HADE and (+)-GADE, as are the signs of the VCD bands in the 1120−1090 $cm^{-1}$ region. Thus, discrimination between (+)-HADE and (+)-GADE (hence, between the diastereomers (2*S*,3*R*)-**3** and (2*S*,3*S*)-**3**) can be realized from experimental VCD spectra, unlike the experimental ECD and ORD spectra. However, the discrimination between two of the diastereomers, (2*S*,3*R*)-**3** and (2*S*,3*S*)-**3**, alone is not sufficient to yield unequivocal absolute configuration assignment from VCD because it is also necessary to verify if VCD can discriminate between the diastereomeric pair (2*S*,3*R*)-**3** and (2*R*,3*R*)-**3** and between (2*S*,3*S*)-**3** and (2*R*,3*S*)-**3** (vide infra).

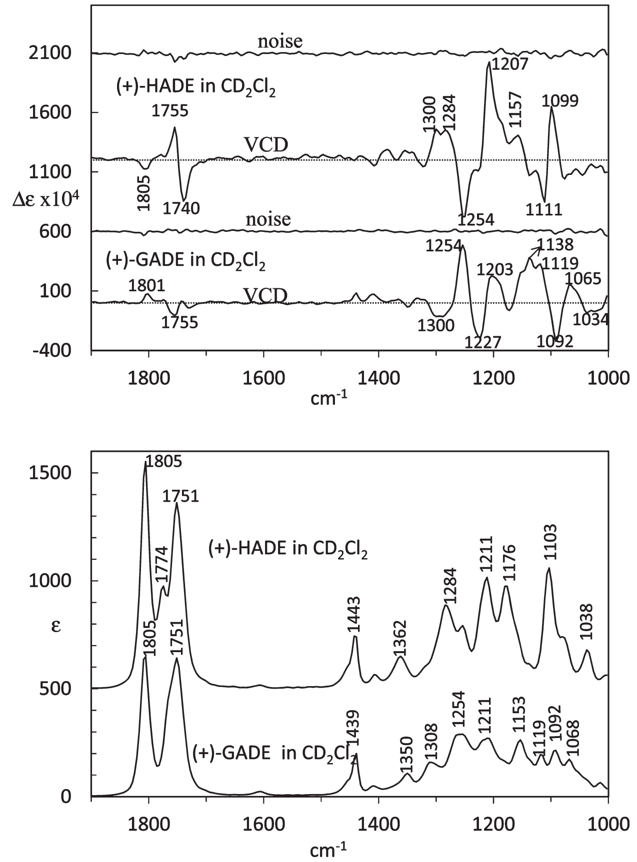

**Figure 3.** Experimental VA (bottom panel) VCD (top panel) spectra for (+)-HADE and (+)-GADE in $CH_2Cl_2$.

The predicted population-weighted VA and VCD spectra for (2*S*,3*R*)-**3** at the B3LYP/aug-cc-pVDZ-PCM level are shown in Figure 4, and those obtained in the B3LYP/aug-cc-pVDZ calculation are provided as Supporting Information. The predicted VA and VCD spectra for (2*S*,3*R*)-**3** at the B3LYP/aug-cc-pVDZ-PCM level are found to have excellent correlation to the corresponding experimental spectra of (+)-HADE (see Figure 4). This correlation becomes poor at the B3LYP/aug-cc-pVDZ level (see Supporting Information) because gas phase predicted vibrational band positions deviate significantly from the observed band positions in $CD_2Cl_2$ solution. This observation reemphasizes our previous observation[11] that the recent implementation of PCM[19,20] significantly enhances the correlation between solution-phase calculated VA and VCD spectra and the corresponding experimental spectra in solution.

The excellent correlation, as seen in Figure 4, between the experimental VA/VCD spectra of (+)-HADE and calculated VA/VCD spectra for (2*S*,3*R*)-**3** may be used to confirm the known configuration, (+)-(2*S*,3*R*)-HADE. A similar correlation between experimental VA/VCD spectra of (+)-GADE and calculated VA/VCD spectra for (2*S*,3*S*)-**3** was used recently[14] to confirm the known configuration as (+)-(2*S*,3*S*)-GADE. However, to validate these conclusions, it is necessary to show that a similar correlation, or even a resemblance of possible correlation, does not exist between the experimental VCD spectra and those calculated for the two other diastereomers; namely, the

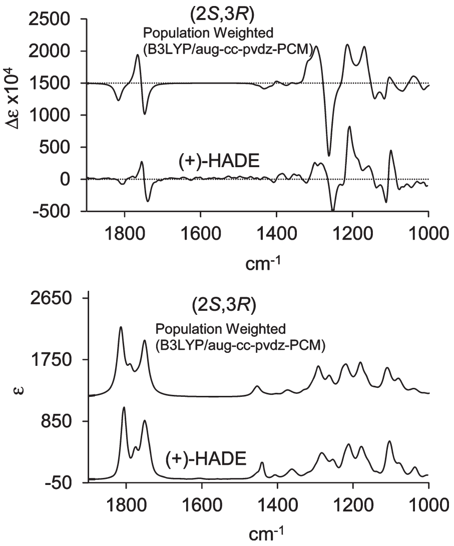

**Figure 4.** Comparison of experimental VA (bottom panel) and VCD (top panel) spectra for (+)-HADE in $CH_2Cl_2$ with predicted population-weighted spectra at the B3LYP/aug-cc-pVDZ-PCM level for (2*S*,3*R*)-**3**.

(2*R*,3*S*) and (2*R*,3*R*) stereoisomers. For this purpose, the experimental VA/VCD spectra of (+)-HADE and (+)-GADE are compared with those calculated at the B3LYP/aug-cc-pVDZ-PCM level for all four diastereomers in Figure 5. Note that the calculated spectra for the (2*R*,3*S*) and (2*R*,3*R*) configurations can be obtained by multiplying the calculated spectra for (2*S*,3*R*) and (2*S*,3*S*), respectively, by −1. The correlation between experimental and calculated VCD bands is displayed using double-headed arrows in Figure 5. From this correlation, it can be noted that the experimental VCD spectra of (+)-HADE can be correlated to the calculated spectra of not only the (2*S*,3*R*) configuration but also the (2*R*,3*R*) configuration. Although the correlation of the VCD spectrum of (+)-HADE with that of the (2*R*,3*R*) configuration is not as strong as that with the (2*S*,3*R*) configuration, the correlation shown in Figure 6 cannot be ruled out, given the uncertainties in quantum chemical calculations for vibrational band positions and intensities. The uncertainties in quantum chemical predictions often arise from variations in predicted energies, populations, band positions and band intensities due to their dependence on the rigor of the quantum chemical method used. Similarly, the experimental VCD spectra of (+)-GADE can be correlated to the calculated spectra of not only the (2*S*,3*S*) configuration but also the (2*R*,3*S*) configuration. Here again, one cannot rule out the possible correlation between the VCD spectra of (+)-GADE and the (2*R*,3*S*) configuration. On the basis of the VCD spectral analysis alone, a safer conclusion to draw is that there are two possibilities for the absolute configuration of (+)-HADE—namely, (2*S*,3*R*) and (2*R*,3*R*)—and two possibilities for the absolute configuration of (+)-GADE—namely, (2*S*,3*S*) and (2*R*,3*S*). These possibilities can be narrowed into unequivocal assignments using the analysis of multiple spectral methods as discussed below.

**Combined Analysis of Spectral Methods.** The inability of a given chiroptical method to determine the absolute configurations of stereoisomers, as noted above, can be overcome if combined analyses of these methods are undertaken. (a) Combined analysis of ECD and VCD: If the absolute configuration of (+)-HADE were not known, then the uncertainty in assigning (2*S*,3*R*) or (2*R*,3*R*) configuration to (+)-HADE on the basis of VCD results alone could be eliminated by noting that the (2*R*,3*R*) configuration is not applicable to (+)-HADE because (+)-HADE exhibits positive ECD in the 190−250 nm region, which is opposite to that predicted for the (2*R*,3*R*) configuration. Similarly, if the absolute configuration of (+)-GADE were not known, the uncertainty in assigning (2*S*,3*S*) or (2*R*,3*S*) configurations to (+)-GADE on the basis of VCD results alone could be eliminated by noting that the (2*R*,3*S*) configuration is not applicable to (+)-GADE because (+)-GADE exhibits positive ECD in the 190−250 nm region, which is opposite to that predicted for the (2*R*,3*S*) configuration. Thus, a combined analysis of ECD and VCD results yields a (2*S*,3*R*) configuration for (+)-HADE and a (2*S*,3*S*) configuration for (+)-GADE, providing a better approach for assigning the absolute configurations of diastereomers (see Table 2). (b) Combined analysis of ORD and VCD: Just as in the combined analysis of ECD and VCD, the (2*R*,3*R*) configuration is not applicable to (+)-HADE because (+)-HADE exhibits positive ORD in the 365−633 nm region, which is opposite in sign to that predicted for the (2*R*,3*R*) configuration. Similarly, the (2*R*,3*S*) configuration is not applicable to (+)-GADE because (+)-GADE exhibits positive ORD

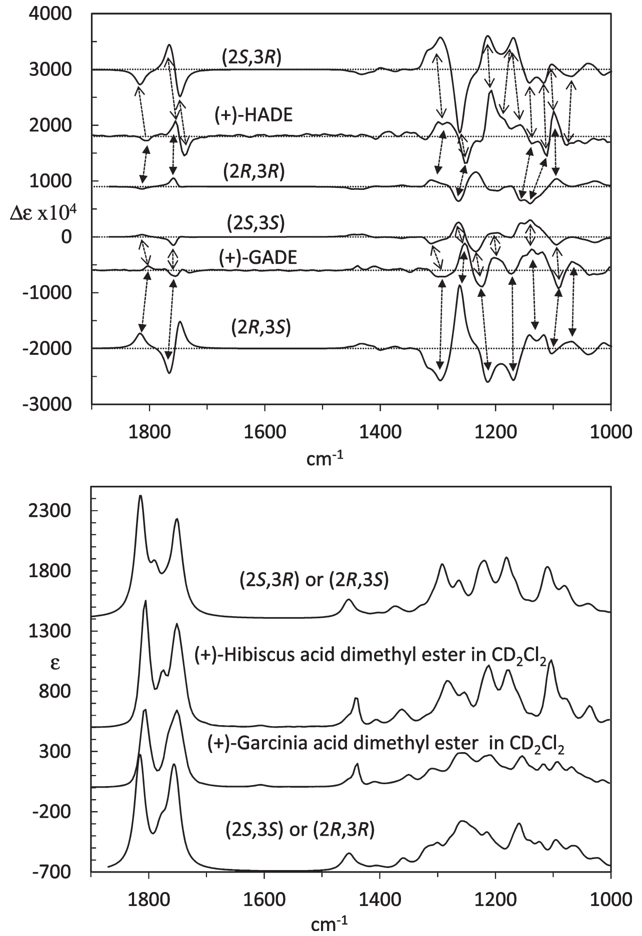

**Figure 5.** Comparison of experimental VA (bottom panel) and VCD (top panel) spectra for (+)-HADE and (+)-GADE in $CH_2Cl_2$ with predicted population-weighted spectra for all four diastereomers ((2*S*,3*R*)-**3**, (2*S*,3*S*)-**3**, (2*R*,3*S*)-**3**, and (2*R*,3*R*)-**3**) at the B3LYP/aug-cc-pVDZ-PCM level.

(in the 365−633 nm region), which is opposite in sign to that predicted for the (2*R*,3*S*) configuration. Thus, a combined analysis of ORD and VCD results yields a (2*S*,3*R*) configuration for (+)-HADE and a (2*S*,3*S*) configuration for (+)-GADE, providing a better approach for assigning the absolute configurations of diastereomers. (c) Special role of unpolarized VA spectra: Even though the unpolarized VA spectra of enantiomers are identical, those of diastereomers need not be. This is evident in Figures 3 and 5. The VA spectra predicted for the enantiomers (2*S*,3*S*) and (2*R*,3*R*) match well with the experimental VA spectrum of (+)-GADE. Similarly, the VA spectra predicted for the enantiomers (2*S*,3*R*) and (2*R*,3*S*) match well with the experimental VA spectrum of (+)-HADE, but the predicted VA spectra of diastereomers (2*S*,3*S*) and (2*S*,3*R*) can be seen in Figure 5 to be significantly different, as also seen in Figure 4 for the experimental VA spectra of (+)-HADE and (+)-GADE. Thus, VA spectra do provide discrimination among diastereomers (2*S*,3*S*) and (2*S*,3*R*) or among their enantiomers (2*R*,3*R*) and (2*R*,3*S*). Then the ambiguities noted during the assignment of absolute configurations of diastereomers based on VCD alone can be avoided (Table 2) if criteria for matching the VA spectral pattern are also imposed along with matching of VCD band signs.

Similar analysis by combining ECD and VA results or ORD and VA results can also be used to discriminate between diastereomers (see Table 2). Thus, we recommend the use of VA spectra, in combination with chiroptical spectra, for differentiation between the diastereomers of chiral compounds.

It should be noted that the combined analysis of ECD and ORD spectra, however, would not have provided diastereomeric discrimination (see Table 2) for the molecules considered here, which is not surprising, since ECD and ORD are not independent methods and are related through Kramers−Kronig transform. Nevertheless, simultaneous investigation of ECD and ORD is recommended for various other reasons.[30]

If the absolute configurations of (+)-HADE and (+)-GADE were not known, then the possible absolute configurations that could be inferred for these two compounds from ECD, ORD, VCD, and VA are summarized in Table 2. It can be seen that the only absolute configuration that is predicted commonly by all of the methods for (+)-HADE is (2*S*,3*R*), and that for (+)-GADE is (2*S*,3*S*). Thus, combined analyses of multiple chiroptical spectroscopic methods can eliminate the uncertainties in assigning the absolute configurations of diastereomers. These observations support our previously made recommendation[30] for the use of more than one chiroptical spectroscopic method for chiral molecular structural determination. In addition, we conclude from the present study that the unpolarized VA spectra can also be quite helpful when uncertainties in the assignment of absolute configurations of diastereomers are not resolved from chiroptical spectral analysis. Although the Raman (and ROA) spectra are not investigated here, it is reasonable to estimate that an advantage similar to that demonstrated here with VA spectra can be realized from the combined analysis of the Raman and chiroptical spectra of diastereomers.

## CONCLUSIONS

Using chioptical spectroscopic investigations on dimethyl esters of hibiscus acid and garcinia acid, it has been noted that a single chiroptical spectroscopic method by itself may not be able to determine the absolute configurations of diastereomers. This is because more than one diastereomer can have similar properties when analyzed with a single chiroptical method. Combined analyses of different chiroptical spectroscopic methods may eliminate the ambiguities in assigning the absolute configurations of diastereomers. It has also been noted that some ambiguities in the assignment of absolute configurations of diasteromers using chiroptical methods can be avoided if the spectral analysis also includes unpolarized VA spectra.

## ASSOCIATED CONTENT

**Supporting Information.** EA and ECD spectra of (2*S*,3*R*)-HADE at the B3LYP/6-31G*, B3LYP/aug-cc-pVDZ, CAM-B3LYP/aug-cc-pVDZ, and B3LYP/aug-cc-pVDZ-PCM levels; ORD spectra of (2*S*,3*R*)-HADE at the B3LYP/6-31G*, B3LYP/aug-cc-pVDZ, CAM-B3LYP/aug-cc-pVDZ, and B3LYP/aug-cc-pVDZ-PCM levels; VA and VCD spectra of (2*S*,3*R*)-HADE at the B3LYP/aug-cc-pVDZ level. This material is available free of charge via the Internet at http://pubs.acs.org

## AUTHOR INFORMATION

### Corresponding Author

*Phone: (615)322-2836. Fax: (615)322-4936. E-mail: Prasad.L.Polavarapu@vanderbilt.edu.

## ACKNOWLEDGMENT

P.L.P gratefully acknowledges NSF funding (CHE-0804301) and helpful communications with Dr. Phil Klunzinger of Wavefunctions Inc., in the use of the SPARTAN program. E.A.D was supported by the Vanderbilt NSF-REU program (CHE 0850976), and E.K.H. was supported by predoctoral traineeships (T32 ES07028). I.I. and D.H. acknowledge the Department of Science and Technology, Government of India, New Delhi, for financial assistance (Project No. SR/S1/OC/54-2007). This work was conducted in part using the resources of the Advanced Computing Center for Research and Education at Vanderbilt University, Nashville, TN.

## REFERENCES

(1) Ibnusaud, I; Thomas, P. T.; Rani, R. N.; Sasi, P. V.; Beena, T.; Hisham, A. *Tetrahedron* **2002**, *58*, 4887–4892.

(2) (a) Lewis, Y. S.; Neelakantan, S.; Anjanamurthy *Curr. Sci.* **1964**, *3*, 82–83. (b) Lewis, Y. S.; Neelakantan, S. *Phytochemistry* **1965**, *4*, 619–625.

(3) Jena, B. S.; Jayaprakasha, G. K.; Singh, R. P.; Sakariah, K. K. *J. Agric. Food Chem.* **2002**, *50*, 10–22.

(4) Boll, P. M.; Sorensen, E.; Balieu, E. *Acta Chem. Scand.* **1969**, *23*, 286–293. Glusker, J. P.; Minkin, J. A.; Soule, F. B. *Acta Crystallogr.* **1972**, *B28*, 2499–2505.

(5) Autschbach, J. *Chirality* **2009**, *21*, E116–E152.

(6) Wilson, S. M.; Wiberg, K. B.; Murphy, M. J.; Vaccaro, P. H. *Chirality* **2008**, *20*, 357–369.

(7) (a) Devlin, F. J.; Stephens, P. J.; Cheeseman, J. R.; Frisch, M. J. *J. Am. Chem. Soc.* **1996**, *118*, 6327–6328. (b) Freedman, T. B.; Cao, X; Dukor, R. K.; Nafie, L. A. *Chirality* **2003**, *15*, 743–758.

(8) (a) Barron, L. D.; Buckingham, A. D. *Chem. Phys. Lett.* **2010**, *492*, 199–213. (b) Ruud, K.; Thorvaldsen, A. J. *Chirality* **2009**, *21*, E54–E67.

(9) For a recent review on VCD applications for natural products, see: Polavarapu, P. L. In *Comprehensive Chiroptical Spectroscopy*; Berova, N., Polavarapu, P. L., Nakanishi, K., Woody, R. W., Eds.; John Wiley, New York, 2011.

(10) The concentrated aqueous extract was washed with hexane. To the aqueous layer, acetone was added to precipitate the insoluble materials. After the evaporation of acetone, NaOH solution (8 N) was added to adjust the pH to 12. Addition of alcohol resulted in the precipitation of the sodium salt of the acid. The pH was further adjusted to 2.0 with HCl (2 N), followed by concentration, which leads to a syrupy mass that was extracted with dry acetone. The acetone extract was concentrated. The thick syrup triturated was further extracted with ether to yield the lactone in the pure form.

(11) Arndt, F. *Org. Synth* **1943**, *Coll. vol. II*, 165–167.

(12) Yoshihara, T.; Ichihara, A.; Nuibe, H.; Sakamura, S.; Sugita, M.; Imamoto, S.; Senoh, S. *Agric. Biol. Chem.* **1974**, *38*, 121–126.

(13) NMR data of synthesized HADE are as follows: $^{1}$H NMR[12] (600 MHz, DMSO-$d_6$) $\delta_{\mathrm{H}}$: 6.80 (1H, s), 5.36 (1H, s), 3.76 (3H, s), 3.68 (3H, s), 3.21 (1H, d, $J$ = 17.4 Hz), 2.68 (1H, d, $J$ = 17.4 Hz). $^{13}$C NMR (150 MHz, DMSO-$d_6$) $\delta_{\mathrm{C}}$: 172.6, 170.7, 166.0, 81.8, 77.8, 53.0, 52.3, 41.4.

(14) Polavarapu, P. L.; Scalmani, G.; Hawkins, E. K.; Rizzo, C.; Jeirath, N.; Ibnusaud, I.; Habel, D.; Nair, D. S.; Haleema, S. *J. Nat. Prod.* **2011**, *74*, 321–328.

(15) Becke, A. D. *J. Chem. Phys.* **1993**, *98*, 5648–5652.

(16) Ditchfield, R.; Hehre, W. J.; Pople, J. A. *J. Chem. Phys.* **1971**, *54*, 724–728.

(17) Kendall, R. A.; Dunning, T. H., Jr.; Harrison, R. J. *J. Chem. Phys.* **1992**, *96*, 6796–6806.

(18) Tomasi, J.; Mennucci, B.; Cammi, R. *Chem. Rev.* **2005**, *105*, 2999–3094. Cossi, M.; Scalmani, G.; Rega, N.; Barone, V. *J. Chem. Phys.* **2002**, *117*, 43–54.

(19) Scalmani, G.; Frisch, M. J. *J. Chem. Phys.* **2010**, *132*, 114110–114124.

(20) Frisch, M. J.; Trucks, G. W.; Schlegel, H. B.; Scuseria, G. E.; Robb, M. A.; Cheeseman, J. R.; Scalmani, G.; Barone, V.; Mennucci, B.; Petersson, G. A.; Nakatsuji, H.; Caricato, M.; Li, X.; Hratchian, H. P.; Izmaylov, A. F.; Bloino, J.; Zheng, G.; Sonnenberg, J. L.; Hada, M.; Ehara, M.; Toyota, K.; Fukuda, R.; Hasegawa, J.; Ishida, M.; Nakajima, T.; Honda, Y.; Kitao, O.; Nakai, H.; Vreven, T.; Montgomery, J. A., Jr.; Peralta, J. E.; Ogliaro, F.; Bearpark, M.; Heyd, J. J.; Brothers, E.; Kudin, K. N.; Staroverov, V. N.; Kobayashi, R.; Normand, J.; Raghavachari, K.; Rendell, A.; Burant, J. C.; Iyengar, S. S.; Tomasi, J.; Cossi, M.; Rega, N.; Millam, J. M.; Klene, M.; Knox, J. E.; Cross, J. B.; Bakken, V.; Adamo, C.; Jaramillo, J.; Gomperts, R.; Stratmann, R. E.; Yazyev, O.; Austin, A. J.; Cammi, R.; Pomelli, C.; Ochterski, J. W.; Martin, R. L.; Morokuma, K.; Zakrzewski, V. G.; Voth, G. A.; Salvador, P.; Dannenberg, J. J.; Dapprich, S.; Daniels, A. D.; Farkas Ö.; Foresman, J. B.; Ortiz, J. V.; Cioslowski, J.; Fox, D. J. *Gaussian 09*; Gaussian, Inc.: Wallingford, CT, 2009.

(21) Caricato, M.; Trucks, G. W.; Frisch, M. J.; Wiberg, K. B. *J. Chem. Theor. Comput.* **2010**, *6*, 370–383.

(22) Yanai, T.; Tew, D. P.; Handy, N. C. *Chem. Phys. Lett.* **2004**, *393*, 51–57.

(23) Georgik, L.; Kruse, H.; Grimme, S. In *Comprehensive Chiroptical Spectroscopy*; Berova, N.; Polavarapu, P. L.; Nakanishi, K.; Woody, R. W. Eds.; John Wiley: New York, 2011.

(24) Rohrdanz, M. A.; Herbert, J. M. J. *Chem. Phys.* **2008**, *129*, 034107.

(25) SPARTAN '08, Wavefunction, Inc., Irvine, CA; www.wavefun.com/products/spartan.html,

(26) Options used with SPARTAN program are CONF_SELECTION_RULE=5, WINDOW=20.0, SEARCHMETHOD=THOROUGH, MMFF94 force field.

(27) Dr. Phil Klunzinger of Wavefunction, Inc. advised that a trick that is sometimes useful with the SPARTAN program to find twisted boat conformations is to select all "waggable" carbon atoms (sp$^3$ carbons not attached to the sp$^3$ centers) and choose a parameter 3 (in the torsion window) for them. This procedure did find conformations with both positive and negative puckering angles for HADE, but not for some other five-membered ring systems. Several literature papers that dealt with five-membered ring systems using the SPARTAN program did not seem to have made use of this option.

(28) *CONFLEX Program*; CONFLEX Corporation: AIOS Meguro 6F, 2-15-19, Kami-Osaki, Shinagawa-ku, Tokyo 141−0021, Japan; www.conflex.us.

(29) The options used with the CONFLEX program are MMFF94S force field, SEL=20.0, SEARCH=ENERGY.

(30) Polavarapu, P. L. *Chirality* **2008**, *20*, 664–672.